Processing and Application of Ceramics 15 [3] (2021) 226–237
https://doi.org/10.2298/PAC2103226P

The effect of lanthanum addition on the microstructure and mechanical properties of Mg-modified hydroxyapatite ceramics

Serdar Pazarlioglu[1,*], Ogulcan Algan[2], Ahmet Mert Isikogullari[2], Hasan Gokce[3]

[1]*Marmara University, Technology Faculty, Metallurgy and Material Science Engineering, Goztepe Campus, Istanbul, Turkey*
[2]*Marmara University, Institute of Pure and Applied Sciences, Goztepe Campus, Istanbul, Turkey*
[3]*İstanbul Technical Üniversite, Adnan Tekin Research Center, Macka Campus, Istanbul, Turkey*

Received 24 November 2020; Received in revised form 6 April 2021; Accepted 13 July 2021

Abstract

In the present paper, the effect of La_2O_3 (0.25, 0.5 and 1 wt.%) addition on the phase stability, porosity, density, hardness, fracture toughness, compressive strength and brittleness index of hydroxyapatite modified with 1 wt.% of MgO was investigated. Hydroxyapatite (HA) without additives sintered at 1300 °C has mixture of dominant hydroxyapatite phase with beta-tricalcium phosphate (β-TCP), alpha-tricalcium phosphate (α-TCP) and calcium oxide (CaO) phases. The microstructure is characterized with transgranular microcracks and oversized grains. Although the density and hardness of the pure HA increased with increasing temperature, a steady decrease in fracture toughness (from 0.96 to 0.71 MPa·m$^{1/2}$) and compressive strength (from 130.2 to 65.6 MPa) was observed. For the HA modified with 1 wt.% of MgO the highest compressive strength (183.2 MPa) and fracture toughness (1.47 MPa·m$^{1/2}$) were obtained at 1200 °C and at this temperature the brittleness index was 3.24 μm$^{-1/2}$. Increase in the sintering temperature led to the increase of the brittleness index of the pure HA, MgO modified HA and La_2O_3-MgO modified HA samples. The addition of 1 wt.% La_2O_3 to 1 wt.% MgO-HA contributed to the increase in the compressive strength of about 10% (from 183.2 to 202.0 MPa), fracture toughness of about 69% (from 1.37 to 2.32 MPa·m$^{1/2}$) and also decrease of the brittleness index from 3.24 to 2.18 μm$^{-1/2}$. The best performance after sintering at 1300 °C was obtained for the MgO-HA sample with 0.25 wt.% La_2O_3. As a result of this study, a new candidate material for biomedical application with superior mechanical properties and the phases that do not cause adverse reactions in the human body could be 1 wt.% MgO-HA modified with 1 wt.% La_2O_3 and sintered at 1200 °C.

Keywords: *hydroxyapatite, magnesium oxide, lanthanum oxide, sintering, mechanical properties*

I. Introduction

Hydroxyapatite (HA) is commonly used as the bulk implant material, bone spacer and/or filler in load-bearing areas of the body, because of its biocompatibility and bioactivity. However, the poor mechanical properties of HA restrict its use in load-bearing applications. Various techniques have been used to increase the poor mechanical properties of HA such as making composites by the addition of inert oxides, and using different pressing/sintering methods (e.g. underwater shock compaction, hot press sintering, and pressureless sintering) [1]. Although the addition of inert oxides such as Al_2O_3 [2], ZrO_2 [3] or TiO_2 [4] to HA contributes to the performance of HA in load-bearing applications, they cause the reduction in its decomposition temperature and bioactivity property. The human body contains different elements, such as Zn, Cu, Fe, Mn, Mg, Ni, Cr, Co, Mo, Se etc. and each of them has different vital importance. Thus, 60–65% of the total amount of Mg in the human body is found in bones and teeth, while the remaining 35–40% is found in muscle tissues, nerves, soft tissues and body fluid. Studies have shown that insufficient Mg causes various problems such as muscle spasms, cardiovascular disease, diabetes, high blood pressure, anxiety disorders, migraine, osteoporosis and cerebral infarction [5,7].

Magnesium oxide is used in a wide range of prod-

*Corresponding author: tel: +90 216 777 39 41,
e-mail: *spazarlioglu@marmara.edu.tr*

ucts such as refractory, paints, paper, plastics, rubber, oil, pharmaceutical, fertilizer, animal feed and the waste treatment agent for neutralizing acids [8]. It is also used as the source to compensate for Mg deficiency in the human body [9]. As stated by Gautam *et al.* [10] MgO modified HA is widely used as bone graft materials due to faster recovery of the host material (bone) by gradually releasing Mg ions from implanted materials. Several studies on binary composites of HA with different amount of MgO have revealed that the addition of 1 wt.% MgO enhances the mechanical properties of HA and promotes its cell attachment [11–14]. It has been also proven that the addition of 1 wt.% MgO also increases thermal stability of HA-based ternary composites [15,16]. However, the addition of higher MgO amount (>1 wt.%) was found to annul the positive effect in HA-ternary composites and cause an increase in the decomposition rate of HA to beta and/or tricalcium phosphate (β- and/or α-TCP) phases. For instance, the addition of 5 wt.% MgO increases the decomposition rate of HA/(10–40 wt.%)ZrO_2 binary composite from 4% to 80% [17]. Human femur bone, which is the part of the body that requires the most load resistance, have a hardness of 4.8 GPa, compressive strength of 100–230 MPa and the fracture toughness of 2–12 MPa·$m^{1/2}$ [18]. However, the properties of HA modified with 1 wt.% MgO are not compatible with human femur bone, as summarized in Table 1.

Recently, it has become attractive to add two different oxide ceramics in the production of HA-based bioceramics. So, we assumed that the mechanical properties of the HA modified with 1 wt.% MgO could be made compatible with human femoral bone by adding an extra material, which has the following properties:

- The melting temperature of the additive material must be lower than MgO in order to increase the densification of 1 wt.% MgO-HA composite.
- The additive material must have an effect on reducing the decomposition rate of 1 wt.% MgO-HA composite.
- The additive material must have a reducing effect on the grain growth of 1 wt.% MgO-HA composite.
- The additive must have a reducing effect on the brittleness index of 1 wt.% MgO-HA composite.

La_2O_3 is one of the materials used in various technological applications such as light-emitting phosphors, solid oxide fuel cells, catalysis, automotive exhaust-gas converters and sorbent materials [25]. In the biomedical industry, it can be used as an optical sensing system for measuring variations in human body temperature and in the magnetic field-controlled targeted release of drugs within the body. It has the ability to suppress bacteria and viruses [26]. La_2O_3 additive in between 0.3 and 2 wt.% both helps to increase the hardness and transverse rupture strength of advanced ceramics (such as B_4C [27], WC [28], etc.) and increase the creep resistance of metallic materials [29]. As stated in previous studies [30,31], the mechanical and physical properties of HA can be made more attractive by adding La_2O_3 for load-bearing applications in the human body. The effect of La_2O_3 additive on HA-ZrO_2 [32], HA-Al_2O_3 [33] and HA-B_2O_3 [34] binary composites was also studied. However, no study has been reported for the co-substitution of MgO and La_2O_3 to HA.

The aim of the present study was to investigate the effect of La_2O_3 additive on microstructure and mechanical properties of HA modified with 1 wt.% MgO. For this purpose, 1 wt.% MgO-HA composites with and without La_2O_3 addition were subjected to sintering between 1100 and 1300 °C and characterized using different techniques.

II. Experimental

2.1. Sample preparation

In the present study HA (commercial purity, Across Organics; Belgium), MgO (99.5% in purity; Sigma Aldrich, USA) and La_2O_3 (99.5% in purity; Sigma Aldrich, USA) powders were used as starting materials. HA was in irregular form with the average grain size of 7.10 μm, MgO and La_2O_3 powders were in spherical form with the average grain size of 3.27 and 3.14 μm, respectively. The starting materials were mixed at 180 rpm for 2 h using a ball milling device in a zirconia coated stainless steel jar with the addition of ethyl alcohol and zirconia balls to prepare the composites, as tabulated in Table 2.

Both zirconia balls and stainless steel container were cleaned with ethyl alcohol to prevent contamination before the mixing process. The mixed powders were dried in an oven at 105 °C for 1 day and then the composite powders at a weight of 1.810 g were pelleted using uniaxial press at 350 MPa to obtain the samples, as in our previous study [35]. Finally, the green bodies were sintered in air at 1100, 1200 and 1300 °C at a ramp rate of 5 °C/min and soaking time of 4 h, and then cooled

Table 1. Properties of HA modified with 1 wt.% MgO - the literature data

Density [g/cm^3]	Hardness [GPa]	Compressive strength [MPa]	Fracture toughness [MPa·$m^{1/2}$]	Ref.
-	7.66	-	1.48	[19]
3.03	-	111.20	1.36	[20]
3.29	3.8	281	-	[21]
-	5.46	-	1.23	[22]
-	4.05	-	0.95	[23]
-	≈6.0	-	≈1.15	[24]

Table 2. Composition of the prepared samples

Sample ID	HA [wt.%]	MgO [wt.%]	La_2O_3 [wt.%]	Total additives [wt.%]
HA	100	-	-	-
HA/1M	99	1	-	1
HA/1M/0.25L	98.75	1	0.25	1.25
HA/1M/0.5L	98.5	1	0.5	1.5
HA/1M/1L	98	1	1	2

to room temperature at a ramp rate of 5 °C/min in air atmosphere.

2.2. Characterization

In order to evaluate the physical and mechanical properties of the sintered samples, theoretical and relative density, porosity, hardness, fracture toughness, brittleness index and compression strength were determined. Sintered density (ρ) and porosity (p) of the samples were calculated by the Archimedes method using Eqs. 1 and 2, respectively:

$$\rho = \frac{Mk}{Ma - Ms} \tag{1}$$

$$p = \frac{Ma - Mk}{Ma - Ms} \times 100 \tag{2}$$

Here Mk is the dry weigh, Ma is the wet weight of the sample and Ms is the wet weight of the suspension in distilled water. Theoretical density (ρ_t) of the sintered samples was calculated using Eq. 3:

$$\rho_t = \frac{m_t}{\left(\frac{m_1}{\rho_1} + \frac{m_2}{\rho_2} + \frac{m_3}{\rho_3}\right)} \tag{3}$$

Here m_t is the total weight of the mixture, m_1 is the weight of HA in the mixture, m_2 is the weight of MgO in the mixture, m_3 is the weight of La_2O_3 in the mixture, whereas ρ_1, ρ_2 and ρ_3 are theoretical densities of HA (3.156 g/cm^3 [36]), MgO (3.580 g/cm^3 [37]) and La_2O_3 (6.510 g/cm^3 [38]), respectively. The relative density (ρ_r) values were determined by Eq. 4:

$$\rho_r = \frac{\rho}{\rho_t} \times 100 \tag{4}$$

The hardness and fracture toughness of each sample were calculated according to our previous study [39]. For hardness and fracture toughness measurements, the samples were firstly ground with 800, 1200 and 2500 mesh SiC paper and then polished with 10, 5, 3 and 1 μm diamond paste until mirror-like surfaces are obtained. They were measured by a Future Tech FM301 microhardness device using loads of 200 and 300 g for 20 and 10 s. The average and standard deviation values were taken from 10 indents. The hardness was calculated by Eq. 5:

$$HV = 1.854\frac{P}{d^2} \tag{5}$$

Here, HV is the hardness, P is the applied force and d is the average indentation diameter. The fracture toughness was calculated by Eq. 6:

$$K_{IC} = 0.203\left(\frac{c}{a}\right)^{-1.5} HV \cdot a^{0.5} \tag{6}$$

Here, K_{IC} is the fracture toughness, c is the radial crack dimension measured from the centre of the indent impression and a is the half diagonal of the indentation.

Compression tests were carried out on ten samples using a universal testing machine (Devotrans FU 50 kN, Turkey) under a loading rate of 2 mm/min. The brittleness index (B) was determined by Eq. 7 [40]:

$$B = \frac{H}{K_{IC}} \tag{7}$$

In order to understand the effect of additive materials on the stability and sintering behaviour of HA, X-Ray diffraction (XRD) and scanning electron microscopy (SEM) examinations were used in the present study. XRD analysis was done by Philips X'Pert machine using Cu Kα as the radiation source in the range of 2θ values between 25° and 50°. The percentage of the phases was determined by the Rietveld analysis. The changes in the surface morphology of the sintered samples were determined by FEI Sirion XL30 SEM machine. The changes in the average grain size of the sintered samples were determined by the linear intercept method.

III. Results and discussion

XRD patterns of hydroxyapatite without additives (the sample HA) sintered at 1100, 1200 and 1300 °C are shown in Fig. 1. The XRD peaks at 2θ of 31.30° are attributed to β-TCP (JCPDS #98-007-6896), which indicates that HA started to partially decompose at 1100 °C. According to the literature, decomposition temperatures of hydroxyapatite range from 700 and 1300 °C [42]. The XRD peaks detected at 2θ position of 30.7° and 37.4° were related to α-TCP (JCPDS #98-007-8499) and CaO (JCPDS #98-003-4977) phases. The decomposition of the HA without additives when it was sintered at 1300 °C can be explained by the following reaction ($Ca_3(PO_4)_2$ is β-TCP, and $Ca_3P_2O_8$ is α-TCP):

$$Ca_{10}(PO_4)_6(OH)_2 \longrightarrow 2\,Ca_3(PO_4)_2 + Ca_3P_2O_8 + CaO + H_2O$$

XRD patterns of hydroxyapatite with 1 wt.% MgO (the sample HA/1M) sintered at 1100, 1200 and 1300 °C

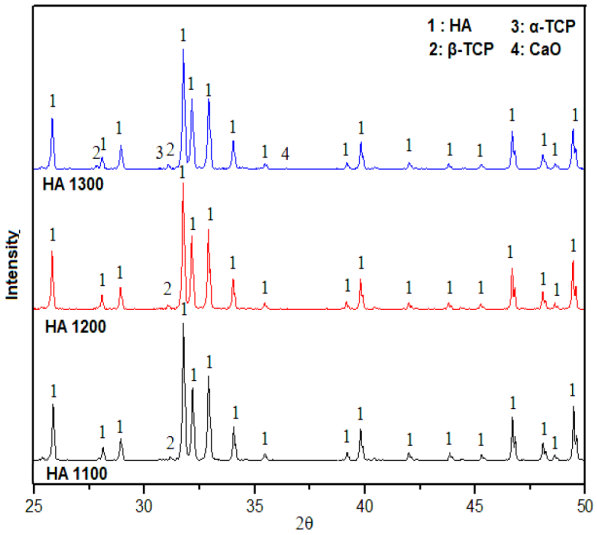

Figure 1. XRD analysis of HA without additives

are shown in Fig. 2. In addition to the dominant HA phase, presence of whitlockite and farringtonite can be seen. The peaks at 2θ of 27.8°, 31.1°, 34.5° and 41.8° were attributed to whitlockite (JCPDS #98-000-0800) and at 2θ of 25.9°, 29.8°, 37.2° and 42.5° to farringtonite (JCPDS #98-001-7130). Whitlockite is formed due to the diffusion of Mg ions into β-TCP [43], as shown in the following reaction:

$$Ca_3(PO_4)_2 + xMgO \longrightarrow Ca_{3-x}Mg_x(PO_4)_2$$

Whitlockite has a hexagonal $R3C$ type crystal lattice structure and provides the stabilization of the β-TCP phase. Therefore, it contributes to the densification, biocompatibility and mechanical properties of HA. Moreover, its solubility in the body is lower than β-TCP [44]. One third of the inorganic part of human bone consists of whitlockite. Whitlockite enhances the osteogenic differentiation and has a negatively charged surface that allows the attraction of osteogenic proteins [45]. So, the co-existence of HA and whitlockite is a desirable association in biomedical applications. The phases of β- and/or α-TCP and CaO detected in the pure HA were generally not detected in both MgO modified HA and MgO-La_2O_3 modified HA. However, in previous studies on HA-MgO [46,47], hydroxyapatite had decomposed to β-TCP, α-TCP and CaO phases. The reason is that the amount of MgO in the related studies was above 1 wt.%. Farringtonite has a monoclinic crystal lattice structure [48]. It exhibits a highly stable behaviour in the body fluid environment and has an accelerating effect on the formation of bone tissues [49,50]. So, it is used in the production of magnesium phosphate cement, which is one of the mineral bone adhesives [51].

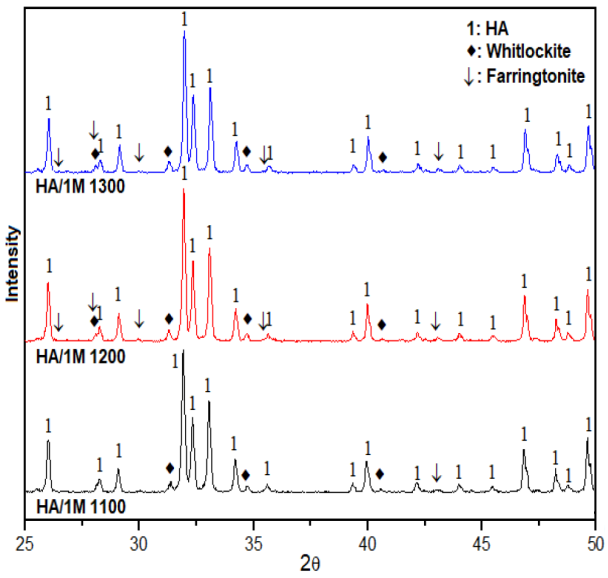

Figure 2. XRD analysis of 1 wt.% MgO-HA composite

XRD patterns of hydroxyapatite with 1 wt.% MgO and addition of La_2O_3 (the samples HA/1M/xL, where x = 0.25, 0.5 and 1) sintered at 1100, 1200 and 1300 °C are shown in Fig. 3. The presence of HA, whitlockite, farringtonite and some La-P-based phases can be detected. These phases are $H_6LaP_3O_6$ (JCPDS #98-005-3428), $LaPO_4$ (JCPDS #98-007-8649), LaP_3O_9 (JCPDS #98-004-3800) and LaP_5O_{14} (JCPDS #98-005-6216). It is seen that La_2O_3 fully reacts with HA, but there is no other phase formed between MgO and La_2O_3. This is due to the dissimilarity of ionic radius of Mg^{2+} (0.72 Å [52]) and La^{3+} (1.16 Å [53]), and also dissimilarity of the distance between Mg–O (1.819 Å [54]) and La–O (2.45 Å [55]). $H_6LaP_3O_6$ was also detected in our previous study when only La_2O_3 added HA had been sintered below 1200 °C [56]. There are four different lanthanum phosphate phases in the La_2O_3-P_2O_5 binary-phase diagram, namely $LaPO_4$ (orthophosphate), $La_2P_4O_{13}$ (tetraphosphate), LaP_3O_9 (metaphosphate/polyphosphate) and LaP_5O_{14} (ultraphosphate) [57]. In the present study, the $La_2P_4O_{13}$ phase has not detected in any HA/1M/xL sample since it forms above 1300 °C. LaP_3O_9 has the base-centred orthorhombic structure [58]. The presence of LaP_3O_9 increases the electrical conductivity of glass-ceramics and accelerates the healing of damaged tissues [59]. $LaPO_4$ forms at temperature above 900 °C as a result of the thermal decomposition of LaP_3O_9 and has a monoclinic crystal structure (space group $P2_1/n$) with the lattice parameters of a = 0.6812 nm, b = 0.7049 nm, c = 0.6484 nm and β = 103.6° [60,62]. It increases the machinability of calcium phosphate ceramics. Because of its chemical stability, non-toxicity and biocompatibility, it can be used in biomedical applications [63,65]. LaP_5O_{14} exhibits a monoclinic structure with space group $P2_1/c$. Unit cell parameters of LaP_5O_{14} are a = 0.878 nm, b = 0.904 nm and c = 1.308 nm [66]. It contributes to the sterilization of biomaterials because it is not affected by UV [67].

Figure 4 shows SEM micrographs with the corresponding average grain sizes of the HA with and without additives. Sintering carried out below 1200 °C

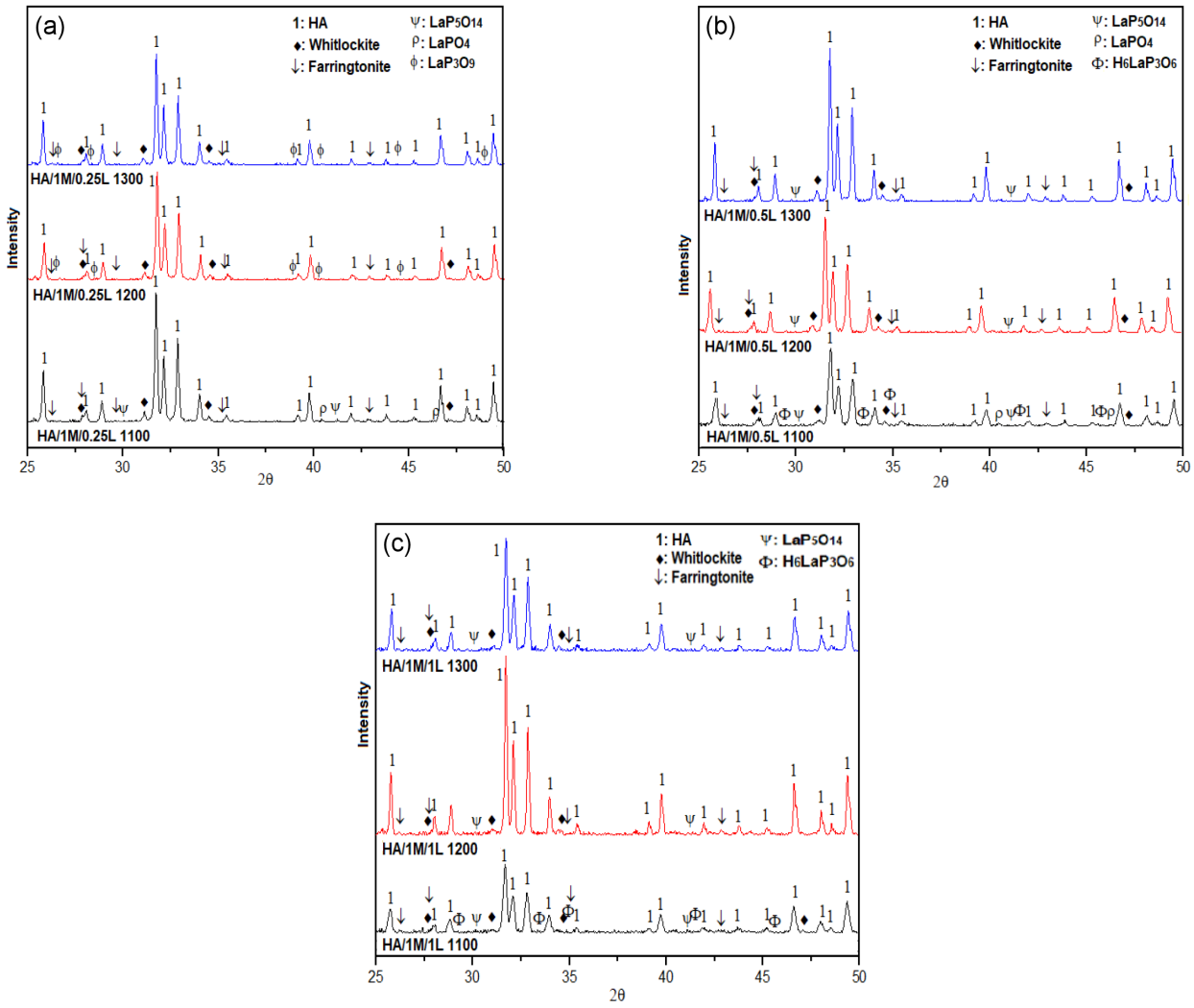

Figure 3. XRD patterns of MgO-La_2O_3 modified HA with addition of: a) 0.25, b) 0.5 and c) 1.0 wt.% La_2O_3

caused porous structures, but when it was above 1200 °C microcracks on the surface were observed. The average grain size of the pure HA was measured as 7.95 and 17.16 µm after sintering at 1200 and 1300 °C, respectively. A reduction in the grain size of 82% and 84% was achieved by the addition of 1 wt.% MgO in comparison to the pure HA after sintering at 1200 and 1300 °C, respectively. This increased to 92% and 94% by the addition of 0.25 wt.% La_2O_3. Microcracks on the surface of HA ceramics are related to three main reasons. The first is the dissimilarity of the thermal expansion coefficient of trace phases with HA [68]. The second is the dissimilarity of crystal lattice structure and/or parameters of trace phases with HA [69]. The third is that the microcracks occur if a critical grain size is exceeded [70]. Microcracks in the MgO modified HA and MgO-La_2O_3 modified samples were also observed when sintering was carried out at 1300 °C. However, not only the intensity but also the size of microcracks in these samples was lower than the pure HA. This is due to two main reasons: i) MgO and La_2O_3 additives prevent the excessive grain growth and ii) whitlockite, farringtonite, LaP_5O_{14} and LaP_3O_9 phases detected in the HA/1M and HA/1M/*x*L samples have the reducing effect on the lattice strain that occurs in HA.

Figure 5 shows changes in the porosity, density and relative density of the HA with and without additives depending on the sintering temperature. The porosity of the HA without additives decreased from 26.58 ± 0.89% to 2.91 ± 0.76%, when the sintering temperature increased to 1300 °C, as shown in Fig. 5a. These values are in good agreement with Yashima *et al.* [71]. The porosity of the HA/1M modified with 1 wt.% MgO was lower than the pure HA at all sintering temperatures. Moreover, La_2O_3 additive contributed to a reduction at around 50% in the porosity of the 1 wt.% MgO-HA, when sintering was carried out at 1200 and 1300 °C. That reduction in the porosity of the sample HA/1M/1L with 1 wt.% La_2O_3 is also higher than in previous studies [72,73].

The density of the pure HA increased from 2.31±0.02 to 3.06±0.02 g/cm^3. The density of the pure HA sintered at 1300 °C is reasonably close to the theoretical density of 3.156 g/cm^3 for the HA ceramics [74]. Its relative

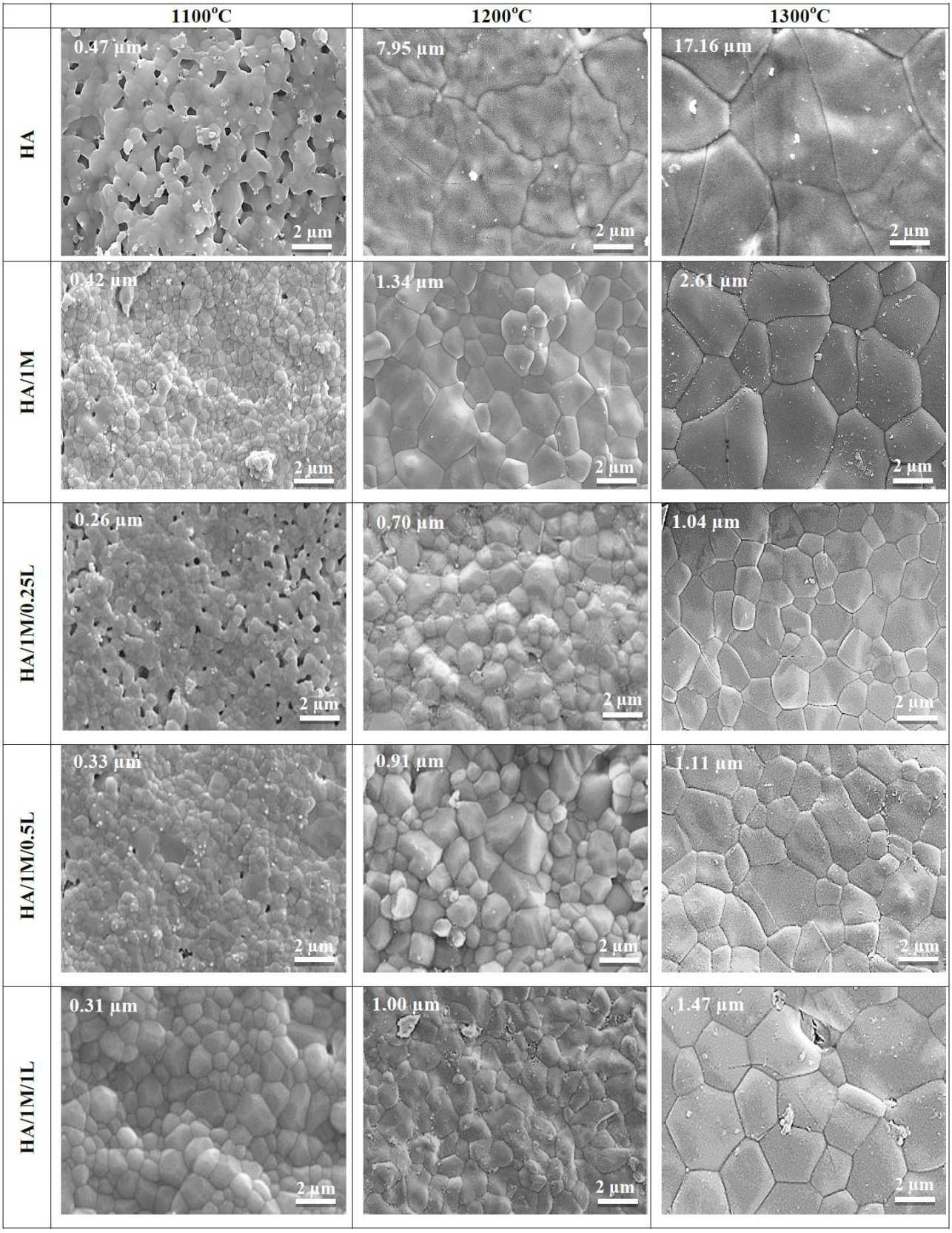

Figure 4. SEM micrographs and the average grain sizes of HA with and without additives

density was 72.42 ± 0.11% at 1100 °C, but increased to 94.99±0.46% at 1200 °C and plateaued at 96.09±0.17% when sintering was carried out at 1300 °C. A plateaued relative density of ~95% was reported by Ruys *et al.* [75]. Figure 5b shows that the densities of the MgO and co-MgO-La_2O_3 added HAs are higher than density of the pure HA at all temperatures. This is due to four main reasons. The first is that not only MgO but also

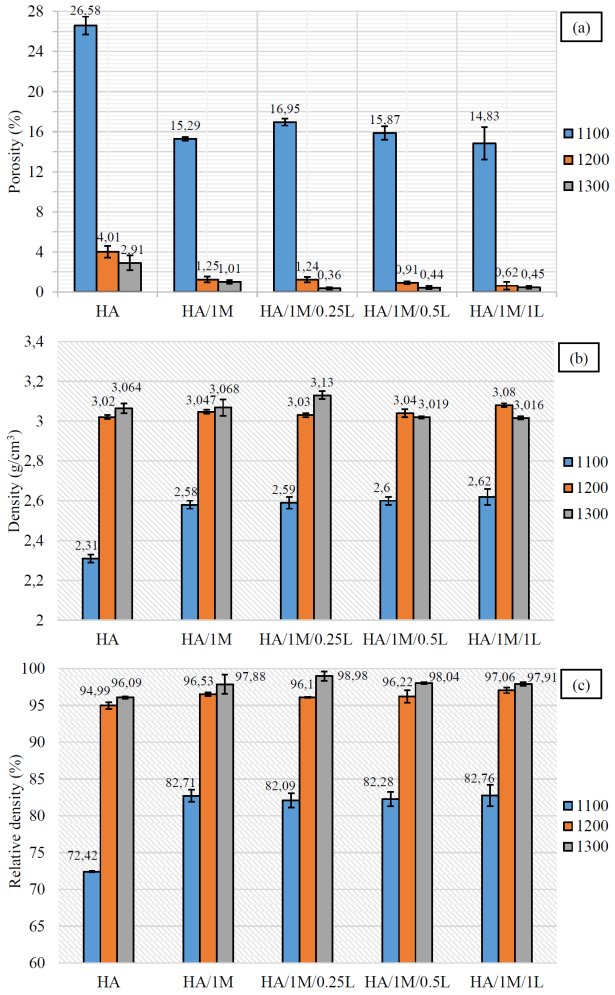

Figure 5. Changes in the (a) porosity, (b) density, and (c) relative density of pure HA and composites depending on the sintering temperatures

MgO-La_2O_3 additives suppress the abnormal growth of HA grains and promote the densification of HA. The second is the stabilization of β-TCP phase by the addition of MgO. The stabilization of β-TCP is advantageous to the sintering because the formation of solid solution restricts the grain growth and eliminates the residual pores along grain boundaries [76]. The third is that secondary phases detected in the pure HA have lower theoretical density values than most of the phases detected in the MgO and co-MgO-La_2O_3 modified HAs (β-TCP: 3.07 g/cm^3 [77], α-TCP: 2.86 g/cm^3 [78], CaO: 3.40 g/cm^3 [79], whitlockite: 3.12 g/cm^3 [80], farringtonite: 2.74 g/cm^3 [81], LaP_5O_{14}: 3.25 g/cm^3 [82], $LaPO_4$: 5.11 g/cm^3 [83], LaP_3O_9: 3.46 g/cm^3 [84]). The fourth is that besides the effect of grain refinement, La_2O_3 addition to the 1 wt.% MgO-HA enhances the sintering activity and diffusion during sintering, thus increasing the density of the MgO-HA sample. La_2O_3 assisted the formation of more dense ceramics due to the inhibition of excessive grain growth [85]. Densification at around 90% is desirable because of the presence of a certain degree of porosity as well as of reabsorbable phases contributing to bone intergrowth and a subsequent implant-bone interfacial adhesion [86]. This has been successfully achieved in the present study.

Figure 6 shows changes in the hardness, fracture toughness, compression strength and brittleness index of the HA with and without additives depending on the sintering temperatures. The hardness of the HA without additives increased from 154.1 ± 5.40 to 499.2 ± 12.39 HV with increase in sintering temperature. Even if the HA without additives is composed of three types of trace phases as shown in Fig. 1, its hardness after sintering at 1200 and 1300 °C is higher than in previous studies [87,88]. This is due to the low porosity, low grain size and low decomposition ratio of HA used in the present study compared to others. As we explained in our previous study, the decomposition ratio of HA in secondary phases was lower than 5% [35] compared to about 40% in other reports [89]. According to Minimum Solid Area (MSA) model that has been proposed by Case *et al.* [90], the increase in porosity leads to lower hardness. The hardness is also correlated to the grain size distribution, according to Hall Petch equation and it increases with the decrease in the grain size distribution [91]. The increase in sintering temperature caused increase in hardness values of the pure HA, MgO modified HA and MgO modified HA with 0.25 and 0.5 wt.% La_2O_3 samples. However, the hardness value of the sample HA/1M/1L with 1.0 wt.% La_2O_3 sintered at 1300 °C was lower than the hardness value at 1200 °C. This is related to two main reasons. The first is the high porous structure of the MgO modified HA with 1 wt.% La_2O_3 compared to other La_2O_3 modified samples. The second is that the introduction of 1 wt.% La_2O_3 into 1 wt.% MgO-HA promoted the bond weakening between grains, when sintering was carried out at 1300 °C. The maximum hardness of the HA without additives was in good agreement with human femur bone, but its mechanical properties decreased with increasing sintering temperature. The hardness of the co-MgO-La_2O_3 modified HAs was also higher than other ternary composites such as HA-ZrO_2-Al_2O_3 [92] and HA-CaO-ZrO_2 [93]. This is due to the both MgO and La_2O_3 additives in amount lower than 5 wt.% inhibit the grain growth of HA compared to ZrO_2, Al_2O_3 and CaO.

The maximum fracture toughness (0.96 ± 0.05 MPa·m$^{1/2}$) and the maximum compressive strength (130.2 ± 6.22 MPa) for the pure HA were measured at 1100 °C. Increment in the sintering temperature led to the reduction in the fracture toughness and compressive strength of the pure HA. The decrease in the mechanical properties of the pure HA with increasing sintering temperature is due to the grain growth and the formation of microcracks. The same behaviour for the pure HA had also been confirmed by Zou and Lee [94]. The fracture toughness of the MgO and co-MgO-La_2O_3 modified HAs firstly increased with increasing sintering temperature and then decreased as in the pure HA. The maximum fracture toughness of the MgO and co-MgO-La_2O_3 modified HAs was obtained at 1200 °C

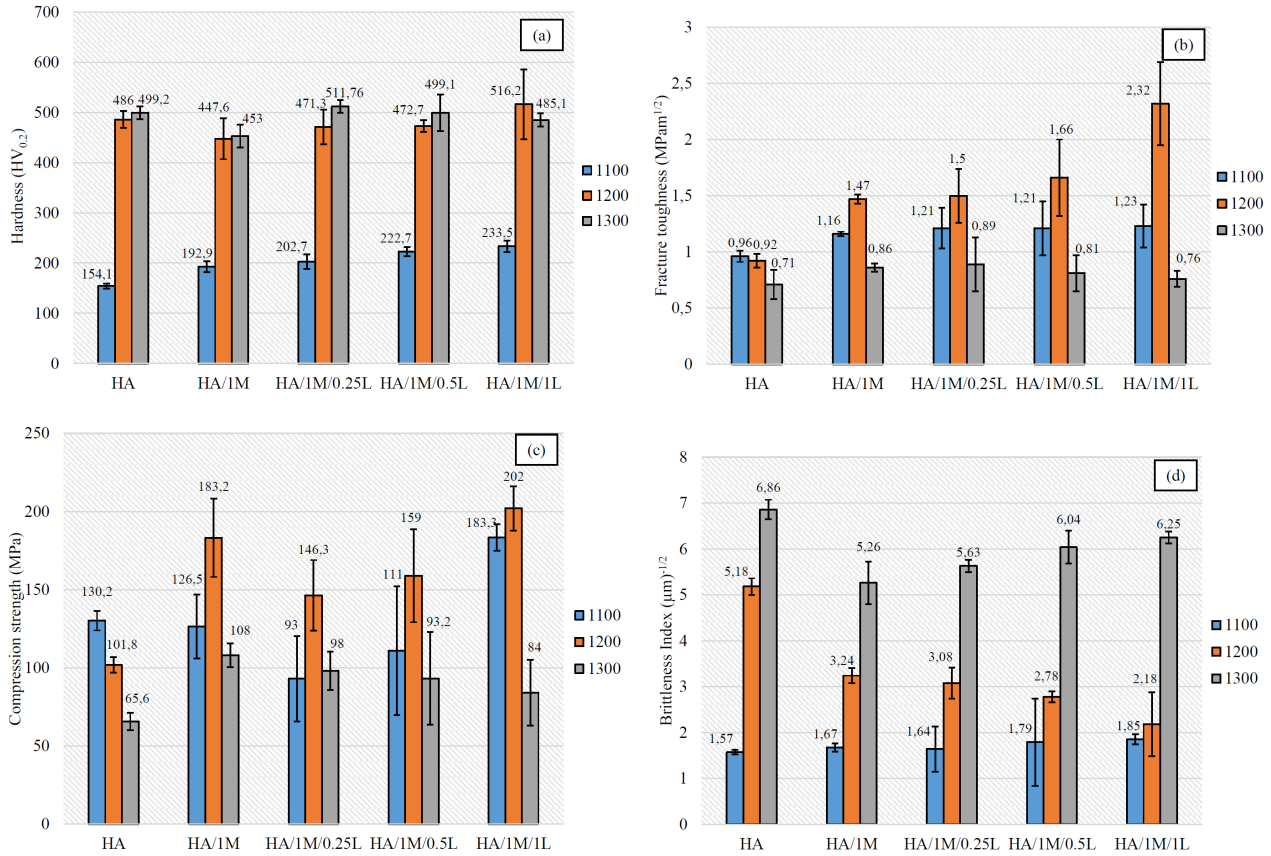

Figure 6. Changes in the (a) hardness, (b) fracture toughness, (c) compression strength, and (d) brittleness index of pure HA and composites depending on the sintering temperatures

as 1.47 ± 0.04, and 2.32 ± 0.67 MPa·m$^{1/2}$, respectively. Although an increment of about 53% was achieved by the addition of 1 wt.% MgO to HA, it cannot be used in the human body due to its fracture toughness value being lower than that of human femur bone. It has become usable in the human body by adding 1 wt.% La_2O_3. The fracture toughness of a material depends on the various parameters, such as: volume fraction, size, shape and properties of phases, grain boundaries, pores and etc. [95]. It is seen that three main factors affect the fracture toughness values in the present study. The first is the double-effect of additives, i.e. while lanthanum phosphate phases mitigate the localized stress concentrations at grain boundaries [96], the migration of Mg^{2+} into β-TCP not only stabilizes the β-TCP phase but also provides resistance to cracking [97]. The second is the inhibition of grain growth in HA by the additives. Smaller grain size improves energy dissipation during indentation [19]. It appears that reduction in the grain size increased the grain-boundary area and the fracture toughness of the pure HA.

The maximum compressive strength of 130.2 ± 6.22 MPa of the pure HA was measured at 1100 °C, but it steadily decreased to 101.8 ± 5.01 and 65.6 ± 5.59 MPa by increasing the sintering temperature. However, a visible increase in the compression strength of HA was achieved by the additions of MgO and MgO-La_2O_3 when it was sintered at 1200 and 1300 °C. The compression strength of 101.8±5.01 MPa of the pure HA obtained at 1200 °C increased to 183.2 ± 25.09 and 202.0 ± 14.14 MPa when it was modified with 1 wt.% MgO and 1 wt.% La_2O_3-1 wt.% MgO, respectively. These values are higher than the compression strength of the pure HA for about 79.96% and 98.42%, respectively. The compression strength of 65.6 ± 5.59 MPa of the pure HA obtained at 1300 °C increased to 108 MPa when it was modified with 1 wt.% MgO. However, the addition of La_2O_3 caused a decrease in the compression strength of the HA/1M sample at 1300 °C. For this temperature, the highest compression strength of 98.0 ± 12.34 MPa was obtained for the sample with 0.25 wt.% La_2O_3. The highest compression strength of 202.0 ± 14.14 MPa obtained for the sample HA/1M/1L with 1 wt.% La_2O_3 is higher than that of other ternary composites in literature [98].

The brittle index displayed an increase with sintering temperature. Although the brittle index of the pure HA attained 6.86 ± 0.21 μm$^{-1/2}$ with increasing temperature, it was lower than that of cold sintered HA [99] and synthetic HA, which were sintered with heating and cooling rate of 10 °C/min [100]. This is because of the two main reasons. The first is the Van der Waals forces have the tendency to slow down the packing of the HAp powder in cold sintering process. The second is that the high

temperature sintering regime causes the high decomposition in HA ceramics. The brittleness index of the MgO and co-MgO-La_2O_3 modified samples was lower than that of the pure HA, when sintering was carried out at 1200 °C. A reduction at about 58% was achieved by increasing the amount of La_2O_3. The brittleness index of $2.18 \pm 0.70\,\mu m^{-1/2}$ obtained for the sample HA/1M/1L with 1 wt.% La_2O_3 is much lower than that of glasses and ceramics, whose values are in the range from 3 to $7\,\mu m^{-1/2}$ [101]. A good machinable dental/bone implant should have a brittleness index lower than $4.3\,\mu m^{-1/2}$, as reported by Linet *et al.* [102]. It is seen that the sample HA/1M/1L with 1 wt.% La_2O_3 sintered at 1200 °C is a candidate material for biomedical applications in which load-bearing is required, because its superior properties and the phases do not cause adverse reactions in the human body.

IV. Conclusions

The effects of La2O3 additive on microstructural and mechanical properties of the HA modified with 1 wt.% of MgO were evaluated by XRD and SEM as well ae by measurements of density, shrinkage, hardness, fracture toughness, brittleness index and compressive strength. The following results were obtained:

- HA without additives exhibit high physical properties and hardness, but its mechanical properties decrease with increasing temperature, and increase its brittleness index.
- Extremely grain growth with the formation of microcracks was observed to the pure HA by increasing temperatures, but they were eliminated by the additives.
- With additions of MgO and MgO-La_2O_3, stress concentrations at grain boundaries were reduced and the migration of Mg^{2+} into β-TCP leads to stabilization of HA.
- It is noted that the samples modified with MgO and La_2O_3 exhibited very high density, implying that the binary sintering additives can effectively promote the densification of HA.
- The mechanical properties of the HA modified with 1 wt.% of MgO was significantly improved in compressive strength (47.7%), and in hardness (39.2%) by the addition of 1 wt.% La_2O_3, when sintering was carried out at 1200 °C.
- The HA modified with 1 wt.% of MgO and 1 wt.% La_2O_3 and sintered at 1200 °C can be used as a biomedical material due to its superior properties, and the phases do not cause adverse reactions in the human body.

References

1. Z. Rezvani, M. Akbari, "Surface modification of hydroxyapatite crystals by Mg-Al-CO_3-layered double hydroxides in HA/Mg-Al-CO_3-LDH nanocomposite", *New J. Chem.*, **39** (2015) 5189–5196.
2. S. Gautier, E. Champion, D. Bernache-Assollant, "Processing, microstructure and toughness of Al_2O_3 platelet-reinforced hydroxyapatite", *J. Eur. Ceram. Soc.*, **17** (1997) 1361–1369.
3. G. Gergely, F. Cinar Sahin, G. Göller, O. Yücel, C. Balázsi, "Microstructural and mechanical investigation of hydroxyapatite-zirconia nanocomposites prepared by spark plasma sintering", *J. Eur. Ceram. Soc.*, **33** (2013) 2313–2319.
4. J. Nie, J. Zhou, X. Huang, L. Wang, G. Liu, J. Cheng, "Effect of TiO_2 doping on densification and mechanical properties of hydroxyapatite by microwave sintering", *Ceram. Int.*, **45** (2019) 13647–13655.
5. F.S. Al-Fartusie, S.N. Mohssan, "Essential trace elements and their vital roles in human body", *Indian J. Adv. Chem. Sci.*, **5** [3] (2017) 127–136.
6. L. Stipniece, K. Salma-Ancane, D. Jakovlevs, N. Borodajenko, L. Berzina-Cimdina, "The study of magnesium substitution effect on physicochemical properties of hydroxyapatite", *Mater. Sci. Appl. Chem.*, **28** (2013) 51–57.
7. L. Morejón-Alonso, C. Mochales, L. Nascimento, W.D. Müller, "Electrochemical deposition of Sr and Sr/Mg-co-substituted hydroxyapatite on Ti-40Nb alloy", *Mater. Lett.*, **248** (2019) 65–68.
8. L.Z. Pei, W.Y. Yin, J.F. Wang, J. Chen, C.G. Fan, Q.F. Zhang, "Low temperature synthesis of magnesium oxide and spinel powders by a sol-gel process", *Mater. Res.*, **13** [3] (2010) 339–343.
9. R. Pournajaf, S.A. Hassanzadeh-Tabrizi, R. Ebrahimi-Kahrizsangi, A. Alhaji, A.A. Nourbakhsh, "Polycrystalline infrared-transparent MgO fabricated by spark plasma sintering", *Ceram. Int.*, **45** (2019) 18943–18950.
10. C.R. Gautam, S. Kumar, S. Biradar, S. Jose, V.K. Mishra, "Synthesis and enhanced mechanical properties of MgO substituted hydroxyapatite: A bone substitute material", *RSC Advances*, **6** (2016) 67565–67574.
11. C.Y. Tan, R. Singh, R. Tolouei, I. Sopyan, W.D. Teng, "Synthesis of high fracture toughness of hydroxyapatite bioceramics", *Adv. Mater. Res.*, **264-265** (2011) 1849–1855.
12. A. Al-Noaman, S.C.F. Rawlinson, R.G. Hill, "The role of MgO on thermal properties, structure and bioactivity of bioactive glass coating for dental implants", *J. Non-Crystal. Solids*, **358** (2012) 3019–3027.
13. M. Khandaker, Y. Li, T. Morris, "Micro and nano MgO particles for the improvement of fracture toughness of bone-cement interfaces", *J. Biomechanics*, **46** (2013) 1035–1039.
14. C.C. Coelho, R. Araújo, P.A. Quadros, S.R. Sousa, F.J. Monteiroa, "Antibacterial bone substitute of hydroxyapatite and magnesium oxide to prevent dental and orthopaedic infections", *Mater. Sci. Eng. C*, **97** (2019) 529–538.
15. A. Bandyopadhyay, S. Bernard, W. Xue, S. Bose, "Calcium phosphate-based resorbable ceramics: Influence of MgO, ZnO, and SiO_2 dopants", *J. Am. Ceram. Soc.*, **89** [9] (2006) 2675–2688.
16. S. Bodhak, S. Bose, A. Bandyopadhyay, "Influence of MgO, SrO, and ZnO dopants on electro-thermal polarization behavior and in vitro biological properties of hydroxyapatite ceramics", *J. Am. Ceram. Soc.*, **94** [4] (2011) 1281–1288.

17. Z. Evis, M. Usta, I. Kutbay, "Hydroxyapatite and zirconia composites: Effect of MgO and MgF_2 on the stability of phases and sinterability", *Mater. Chem. Phys.*, **110** (2008) 68–75.
18. T. Kokubo, H.M. Kim, M. Kawashita, "Novel bioactive materials with different mechanical properties", *Biomaterials*, **24** (2013) 2161–2175.
19. C.Y. Tan, A. Yaghoubi, S. Ramesh, S. Adzila, J. Purbolaksono, M.A. Hassan, M.G. Kutty, "Sintering and mechanical properties of MgO-doped nanocrystalline hydroxyapatite", *Ceram. Int.*, **39** (2013) 8979–8983.
20. S. Kumar, C. Gautam, B.S. Chauhan, S. Srikrishna, R.S. Yadav, S.B. Rai, "Enhanced mechanical properties and hydrophilic behavior of magnesium oxide added hydroxyapatite nanocomposite: A bone substitute material for load bearing applications", *Ceram. Int.*, **46** (2020) 16235–16248.
21. S.J. Kalita, H.A. Bhatt, "Nanocrystalline hydroxyapatite doped with magnesium and zinc: Synthesis and characterization", *Mater. Sci. Eng. C*, **27** (2007) 837–848.
22. H.S. Ryu, K.S. Hong, J.K. Lee, D.J. Kim, J.H. Lee, B.S. Chang, D.H. Lee, C.K. Lee, S.S. Chung, "Magnesia-doped HA/β-TCP ceramics and evaluation of their biocompatibility", *Biomaterials*, **25** (2004) 393–401.
23. M. Lukić, Z. Stojanović, S.D. Škapin, M. Maček-Kržmanc, M. Mitrić, S. Marković, D. Uskoković, "Dense fine-grained biphasic calcium phosphate (BCP) bioceramics designed by two-step sintering", *J. Eur. Ceram. Soc.*, **31** (2011) 19–27.
24. R. Tolouei, S. Ramesh, C.Y. Tan, M. Amiriyan, L. Samuel, B.K. Yap, "Sintering and mechanical properties of MgO-doped hydroxyapatite bioceramics", *Solid State Sci. Technol.*, **19** [2] (2011) 137–143.
25. A.M.A. Mohamed, *Advanced Ceramic Processing*, Intech Open, Croatia, 2015.
26. B. Brabu, S. Haribabu, M. Revathy, S. Anitha, M. Thangapandiyan, K.R. Navaneethakrishnan, C. Gopalakrishnan, S.S. Murugan, T.S. Kumaravel, "Biocompatibility studies on lanthanum oxide nanoparticles", *Toxicol. Res.*, **4** (2015) 1037–1044.
27. Q. Song, Z.H. Zhang, Z.Y. Hu, H. Wang, Y.F. Zhang, X.Y. Li, L.J. Liu, S.L. Li, X.W. Cheng, "Mechanical properties and pre-oxidation behavior of spark plasma sintered B_4C ceramics using (Ti_3SiC_2+CeO_2/La_2O_3) as sintering aid", *Ceram. Int.*, **46** (2020) 22189–22196.
28. X. Ren, Z. Peng, C. Wang, H. Miao, "Influence of nano-sized La_2O_3 addition on the sintering behavior and mechanical properties of WC-La_2O_3 composites", *Ceram. Int.*, **41** (2015) 14811–14818.
29. X. Chen, B. Li, T. Wang, R. Li, J. Wang, S. Ren, G. Zhang, "Strengthening mechanisms of Mo-La_2O_3 alloys processed by solid-solid doping and vacuum hot-pressing sintering", *Vacuum*, **152** (2018) 70–77.
30. M. Shin-Ike, J. Tsutsui, A. Tanaka, S. Murayama, A. Fujita, "Attempts to improve the strength of sintered lanthanum containing hydroxyapatites", *J. Osaka Odontol. Soc.*, **52** (1989) 854–861.
31. A. Tanaka, Y. Nishimura, T. Sakaki, A. Fujita, T. Shin-Ike, "Histologic evaluation of tissue response to sintered lanthanum containing hydroxyapatites subcutaneously implanted in rats", *J. Osaka Dent. Univ.*, **23** (1989) 111–120.
32. S. Khoshsima, B. Yilmaz, A. Tezcaner, Z. Evis, "Structural, mechanical and biological properties of hydroxyapatite-zirconia lanthanum oxide composites", *Ceram. Int.*, **42** (2016) 15773–15779.
33. S. Pazarlioglu, S. Salman, "Effect of lanthanum oxide additive on the sinterability, physical/mechanical, and bioactivity properties of hydroxyapatite-alpha alumina composite", *J. Aust. Ceram. Soc.*, **55** [4] (2019) 1195–1209.
34. S. Khoshsima, A.Z. Alshemary, A. Tezcaner, S. Surdem, Z. Evis, "Impact of B_2O_3 and La_2O_3 addition on structural, mechanical and biological properties of hydroxyapatite", *Process. Appl. Ceram.*, **12** [2] (2018) 143–152.
35. S. Pazarlıoglu, S. Salman, "Sintering effect on the microstructural, mechanical, and in vitro bioactivity properties of a commercially synthetic hydroxyapatite", *J. Aust. Ceram. Soc.*, **53** (2017) 391–401.
36. J. Majling, P. Znáik, A. Palová, S. Svetík, S. Kovalík, D.K. Agrawal, R. Roy, "Sintering of the ultrahigh pressure densified hydroxyapatite monolithic xerogels", *J. Mater. Res.*, **12** [1] (1997) 198–202.
37. H. Abdizadeh, R. Ebrahimifard, M.A. Baghchesara, "Investigation of microstructure and mechanical properties of nano MgO reinforced Al composites manufactured by stir casting and powder metallurgy methods: A comparative study", *Compos. Part B Eng.*, **56** (2014) 217–221.
38. J. Kwon, M. Dai, M.D. Halls, E. Langereis, Y.J. Chabal, R.G. Gordon, "In situ infrared characterization during atomic layer deposition of lanthanum oxide", *J. Phys. Chem. C*, **113** (2009) 654–660.
39. S. Pazarlioglu, S. Salman, "The effect of alumina additive and sintering temperature on the microstructural, physical, mechanical, and bioactivity properties of hydroxyapatite-alumina composites", *J. Austr. Ceram. Soc.*, **56** (2020) 413–431.
40. A. Pandey, V.K. Nigam, K. Balani, "Multi-length scale tribology of hydroxyapatite reinforced with ceria and silver", *Wear*, **404-405** (2018) 12–21.
41. P. Terzioğlu, H. Öğüt, A. Kalemtaş, "Natural calcium phosphates from fish bones and their potential biomedical applications", *Mater. Sci. Eng. C*, **91** (2018) 899–911.
42. H. Li, K.A. Khor, V. Chow, P. Cheang, "Nanostructural characteristics, mechanical properties, and osteoblast response of spark plasma sintered hydroxyapatite", *J. Biomedical Mater. Res. A*, **82** [2] (2007) 296–303.
43. X. Guo, X. Liu, H. Gao, X. Shi, N. Zhao, Y. Wang, "Hydrothermal growth of whitlockite coating on β-tricalcium phosphate surfaces for enhancing bone repair potential", *J. Mater. Sci. Tehnol.*, **34** (2018) 1054–1059.
44. M. Trabelsi, I. AlShahrani, H. Algarni, F. Ben Ayed, E.S. Yousef, "Mechanical and tribological properties of the tricalcium phosphate-magnesium oxide composites", *Mater. Sci. Eng. C*, **96** (2019) 716–729.
45. D. Bellucci, A. Sola, R. Salvatori, A. Anesi, L. Chiarini, V. Cannillo, "Role of magnesium oxide and strontium oxide as modifiers in silicate-based bioactive glasses: Effects on thermal behaviour, mechanical properties and in-vitro bioactivity", *Mater. Sci. Eng. C*, **72** (2017) 566–575.
46. T. Kanazawa, T. Umegaki, K. Yamashita, H. Monma, T. Hiramatsu, "Effects of additives on sintering and some properties of calcium phosphates with various Ca/P ratios", *J. Mater. Sci.*, **26** (1991) 417–422.
47. S. Kobayashi, T. Murakoshi, "Effects of MgO addition on sintering of calcium phosphate ceramics and composites", *Adv. Composite Mater.*, **24** [S1] (2015) 137–146.
48. J.S. Boesenberg, R.H. Hewins, "An experimental investi-

gation into the metastable formation of phosphoran olivine and pyroxene", *Geochim. Cosmochim. Acta*, **74** (2010) 1923–1941.
49. A. Seyfoori, Sh. Mirdamadi, A. Khavandi, Z. Seyed Raufi, "Biodegradation behavior of micro-arc oxidized AZ31 magnesium alloys formed in two different electrolytes", *Appl. Surface Sci.*, **261** (2012) 92–100.
50. B. Kanter, A. Vikman, T. Brückner, M. Schamel, U. Gbureck, A. Ignatius, "Bone regeneration capacity of magnesium phosphate cements in a large animal model", *Acta Biomater.*, **69** (2018) 352–361.
51. T. Brückner, M. Meininger, J. Groll, A.C. Kübler, U. Gbureck, "Magnesium phosphate cement as mineral bone adhesive", *Materials*, **12** (2019) 3819.
52. R. Bhattacharyya, S. Das, S. Omar, "High ionic conductivity of Mg^{2+}-doped non-stoichiometric sodium bismuth titanate", *Acta Mater.*, **159** (2018) 8–15.
53. C. Madhuri, K. Venkataramana, J. Shanker, C.V. Reddy, "Effect of La^{3+}, Pr^{3+}, and Sm^{3+} triple-doping on structural, electrical, and thermal properties of ceria solid electrolytes for intermediate temperature solid oxide fuel cells", *J. Alloys Compd.*, **849** (2020) 156636.
54. P. Batra, R. Gaba, U. Issar, R. Kakkar, "Structures and stabilities of alkaline earth metal oxide nanoclusters: A DFT study", *J. Theoret. Chem.*, **2013** (2013) 720794.
55. J.H. Lin, M.Z. Su, K. Wurst, E. Schweda, "The structure of $La_{26}(BO_3)_8O_{27}$: A structure with a distorted fluorite type arrangement of atoms", *J. Solid State Chem.*, **126** (1996) 287–291.
56. Y. Bozkurt, S. Pazarlioglu, H. Gokce, I. Gurler, S. Salman, "Hydroxyapatite lanthanum oxide composites", *Acta Phys. Polonica A*, **127** (2015) 1407–1409.
57. S.R. Phadke, J.C. Nino, "Conductivity enhancement in lanthanum phosphates", *J. Am. Ceram. Soc.*, **94** [6] (2011) 1817–1823.
58. M.T. Colomer, "Effect of Sr^{2+} doping on sintering behavior, microstructural development and electrical properties of $LaPO_4 \cdot nH_2O$ nanorods prepared by dry mechanical milling", *Int. J. Hydrogen Energy*, **43** [29] (2018) 13462–13474.
59. G. Zhang, R. Yu, L.C. DeJonghe, "Proton conduction in glass-ceramic $La(PO_3)_3$-$Ca(PO_3)_2$". *212th ECS Meeting*, Washington DC, USA, October 7-12, 2007, *ECS Meeting Abstracts*, 774.
60. M. Ferhi, K. Horchani-Naifer, M. Férid, "Combustion synthesis and luminescence properties of $LaPO_4$: Eu (5%)", *J. Rare Earths*, **27** [2] (2009) 182–186.
61. S.S. Sujith, S.L. Arun Kumar, K.V. Mahesh, A. Peer Mohamed, S. Ananthakumar, "Sintering and thermal shock resistance properties of $LaPO_4$ based composite refractories", *Trans. Indian Ceram. Soc.*, **73** [2] (2014) 161–164.
62. J. Yang, X. Jia, X. Zeng, L. Zhu, Z. Chen, "Polyacrylamide gel synthesis, structure and optical properties of LaP_3O_9:Eu^{3+} phosphors", *J. Mater. Sci.*, **50** (2015) 4405–4411.
63. R. Ghosh, S. Pal, R. Sarkar, "Study on the development of machinable hydroxyapatite-yttrium phosphate composite for biomedical applications", *Trans. Indian Ceram. Soc.*, **73** [2] (2014) 121–125.
64. R. Ghosh, R. Sarkar, S. Paul, "Development of machinable hydroxyapatite-lanthanum phosphate composite for biomedical applications", *Mater. Design*, **106** (2016) 161–169.
65. C. Ergun, H. Liu, T.J. Webster, "Osteoblast adhesion on novel machinable calcium phosphate/lanthanum phosphate composites for orthopedic applications", *J. Biomedical Mater. Res. Part A*, **89A** (2009) 727–733.
66. I. Hammas, K. Horchani-Naifer, M. Férid, "Conduction properties of condensed lanthanum phosphates: $La(PO_3)_3$ and LaP_5O_{14}", *J. Rare Earths*, **28** [3] (2010) 321–328.
67. S. Hachani, B. Moine, A. El-akrmi, M. Férid, "Energy transfers between Sm^{3+} and Eu^{3+} in YPO_4, LaP_5O_{14} and LaP_3O_9 phosphates. Potential quantum cutters for red emitting phosphors", *J. Luminescence*, **130** (2010) 1774–1783.
68. E.D. Case, I.O. Smith, M.J. Baumann, "Microcracking and porosity in calcium phosphates and the implications for bone tissue engineering", *Mater. Sci. Eng. A*, **390** (2005) 246–254.
69. H.B. Guo, X. Miao, Y. Chen, P. Cheang, K.A. Khor, "Characterization of hydroxyapatite- and bioglass-316L fibre composites prepared by spark plasma sintering", *Mater. Lett.*, **58** (2004) 304–307.
70. T.P. Hoepfner, E.D. Case, "An estimate of the critical grain size for microcracks induced in hydroxyapatite by thermal expansion anisotropy", *Mater. Lett.*, **58** (2004) 489–492.
71. W. Suchanek, M. Yashima, M. Kakihana, M. Yoshimura, "Hydroxyapatite/hydroxyapatite-whisker composites without sintering additives: Mechanical properties and microstructural evolution", *J. Am. Ceram. Soc.*, **80** [11] (1997) 2805–2813.
72. N. Demirkol, M. Turan, "Production and characterization of ternary sheep hydroxyapatite (SHA)-wollastonite (W)-commercial inert glass (CIG) biocomposite", *Res. Eng. Struct. Mater.*, **5** [2] (2019) 167–174.
73. B. Bulut, N. Demirkol, Z.E. Erkmen, E.S. Kayalı, "Characterization and bioactivity of hydroxyapatite ZrO_2 composites with commercial inert glass CIG addition", *Key Eng. Mater.*, **631** (2015) 166–172.
74. P.Y. Chen, S.F. Wang, R.R. Chien, C.S. Tu, K.C. Feng, C.S. Chen, K.Y. Hung, V.H. Schmidt, "Evolution of the microstructural and mechanical properties of hydroxyapatite bioceramics with varying sintering temperature", *Ceram. Int.*, **45** (2019) 16226–16233.
75. A.J. Ruys, M. Wei, C.C. Sorrell, M.R. Dickson, A. Brandwood, B.K. Milthorpe, "Sintering effects on the strength hydroxyapatite", *Biomaterials*, **16** (1995) 409–415.
76. K. İtatani, M. Takahashi, F.S. Howell, M. Aizawa, "Effect of metal-oxide additions on the sintering of β-calcium orthophosphate", *J. Mater. Sci. Mater. Med.*, **13** (2002) 707–713.
77. N. Ahmad, K. Tsuru, M.L. Munar, M. Maruta, S. Matsuya, K. Ishikawa, "Effect of precursor's solubility on the mechanical property of hydroxyapatite formed by dissolution-precipitation reaction of tricalcium phosphate", *Dental Mater. J.*, **31** [6] (2012) 995–1000.
78. I.M. Hung, W.J. Shih, M.H. Hon, M.C. Wang, "The properties of sintered calcium phosphate with [Ca]/[P] = 1.50", *Int. J. Mol. Sci.*, **13** (2012) 13569–13586.
79. V.V. Smirnov, S.M. Barinov, A.S. Fomin, L.I. Shvorneva, N.S. Sergeeva, "Low temperature calcium carbonate ceramic", *Inorg. Mater. Appl. Res.*, **1** [2] (2010) 143–148.
80. C. Calvo, R. Gopal, "The crystal structure of whitlockite from the Palermo quarry", *Am. Mineral.*, **60** (1975) 120–133.
81. R. Gelli, L. Mati, F. Ridi, P. Baglioni, "Tuning the proper-

ties of magnesium phosphate-based bone cements: Effect of powder to liquid ratio and aqueous solution concentration", *Mater. Sci. Eng. C*, **95** (2019) 248–255.
82. S. Phadke, "Crystallochemical avenues for the enhancement of proton conduction in ceramics: phosphate compounds, experiments and simulation", *Ph.D. thesis*, University of Florida, 2010.
83. T. Anfimova, Q. Li, J.O. Jensen, N.J. Bjerrum, "Thermal stability and proton conductivity of rare earth orthophosphate hydrates", *Int. J. Electrochem. Sci.*, **9** (2014) 2285–2300.
84. $La(PO_3)_3$ (LaP_3O_9) Crystal Structure: Datasheet from "PAULING FILE Multinaries Edition - 2012" in Springer Materials. Eds P. Villars, K. Cenzual, Springer-Verlag GmbH, Heidelberg, 2012.
85. N. Wang, X. Zhang, Z. Bai, "Fabrication of highly transparent Er^{3+}, Yb^{3+}:Y_2O_3 ceramics with La_2O_3/ZrO_2 as sintering additives and the near-infrared and upconversion luminescence properties", *J. Alloys Compd.*, **842** (2020) 155932.
86. V.V. Silva, R.Z. Domingues, F.S. Lameiras, "Microstructural and mechanical study of zirconia-hydroxyapatite (ZH) composite ceramics for biomedical applications", *Composite Sci. Technol.*, **61** (2001) 301–310.
87. I.R. Gibson, S. Ke, S.M. Best, W. Bonfield, "Effect of powder characteristics on the sinterability of hydroxyapatite powders", *J. Mater. Sci. Mater. Med.*, **12** (2001) 163–171.
88. S. Ramesh, C.Y. Tan, R. Tolouei, M. Amiriyan, J. Purbolaksono, I. Sopyan, W.D. Teng, "Sintering behavior of hydroxyapatite prepared from different routes", *Mater. Design*, **34** (2012) 148–154.
89. T.P. Hoepfner, E.D. Case, "The influence of the microstructure on the hardness of sintered hydroxyapatite", *Ceram. Int.*, **29** (2003) 699–706.
90. R.K. Chadha, A.P. Singh, K.L. Singh, C. Sharma, V. Naithani, "Influence of microwave processing and sintering temperature on the structure and properties of Sr/Zr doped hydroxyapatite", *Mater. Chem. Phys.*, **223** (2019) 319–324.
91. L.G. Yu, K.A. Khor, H. Li, P. Cheang, "Effect of spark plasma sintering on the microstructure and in vitro behavior of plasma sprayed HA coatings", *Biomaterials*, **24** (2003) 2695–2705.
92. I. Mobasherpour, M. Solati Hashjin, S.S. Razavi Toosi, R. Darvishi Kamachali, "Effect of the addition ZrO_2-Al_2O_3 on nanocrystalline hydroxyapatite bending strength and fracture toughness", *Ceram. Int.*, **35** (2009) 1569–1574.
93. Z.L. Htun, N. Ahmad, A.A. Thant, A.F.M. Noor, "Characterization of CaO-ZrO_2 reinforced Hap biocomposite for strength and toughness improvement", *Procedia Chem.*, **19** (2016) 510–516.
94. H. Zhou, J. Lee, "Nanoscale hydroxyapatite particles for bone tissue engineering", *Acta Biomater.*, **7** (2011) 2769–2781.
95. S. Yadav, S. Sarkar, A. Aggarwal, A. Kumar, K. Biswas, "Wear and mechanical properties of novel $(CuCrFeTiZn)_{100-x}Pb_x$ high entropy alloy composite via mechanical alloying and spark plasma sintering", *Wear*, **410-411** (2018) 93–109.
96. W. Ruigang, P. Wei, C. Jian, F. Minghao, C. Zhenzhu, L. Yongming, "Synthesis and sintering of $LaPO_4$ powder and its application", *Mater. Chem. Phys.*, **79** (2003) 30–36.
97. E. Babaie, Y. Ren, S.B. Bhaduri, "Microwave sintering of fine grained MgP and Mg substitutes with amorphous tricalcium phosphate: Structural, and mechanical characterization", *J. Mater. Res.*, **31** [8] (2016) 995–1003.
98. S. Mirza, I. Zia, R. Jolly, S. Kazmi, M. Owais, M. Shakir, "Synergistic combination of natural bioadhesive bael fruit gum and chitosan/nano-hydroxyapatite: A ternary bioactive nanohybrid for bone tissue engineering", *Int. J. Bio. Macromol.*, **119** (2018) 215–224.
99. D.O. Obada, E.T. Dauda, J.K. Abifarin, D. Dodoo-Arhin, N.D. Bansod, "Mechanical properties of natural hydroxyapatite using low cold compaction pressure: Effect of sintering temperature", *Mater. Chem. Phys.*, **239** (2020) 122099.
100. A. Bianco, I. Cacciotti, M. Lombardi, L. Montanaro, E. Bemporad, M. Sebastiani, "F-substituted hydroxyapatite nanopowders: Thermal stability, sintering behaviour and mechanical properties", *Ceram. Int.*, **36** (2010) 313–322.
101. S.L. Shi, W. Pan, "Machinable Ti_3SiC_2/hydroxyapatite bioceramic composites by spark plasma sintering", *J. Am. Ceram. Soc.*, **90** [10] (2007) 3331–3333.
102. A. Alinda Shaly, G. Hannah Priya, J. Mary Linet, "An outlook on the mechanical attributes and load curve analysis of hydrothermally acquired hydroxyapatite bioceramic nanoparticles", *Physica B*, **590** (2020) 412223.